Atmospheric evidence for a global secular increase in carbon isotopic discrimination of land photosynthesis

Ralph F. Keeling[a,1], Heather D. Graven[b,c], Lisa R. Welp[d], Laure Resplandy[a], Jian Bi[a], Stephen C. Piper[a], Ying Sun[e], Alane Bollenbacher[a], and Harro A. J. Meijer[f]

[a]Scripps Institution of Oceanography, University of California, San Diego, CA 92093-0244; [b]Department of Physics, Imperial College London, London SW7 2AZ, United Kingdom; [c]Grantham Institute, Imperial College London, London SW7 2AZ, United Kingdom; [d]Earth, Atmospheric, and Planetary Sciences, Purdue University, West Lafayette, IN 47907-2051; [e]School of Integrative Plant Science, Cornell University, Ithaca, NY 14850; and [f]Center for Isotope Research, University of Groningen, 9747AG Groningen, The Netherlands

Edited by Mark H. Thiemens, University of California, San Diego, La Jolla, CA, and approved August 10, 2017 (received for review November 23, 2016)

A decrease in the $^{13}C/^{12}C$ ratio of atmospheric CO_2 has been documented by direct observations since 1978 and from ice core measurements since the industrial revolution. This decrease, known as the ^{13}C-Suess effect, is driven primarily by the input of fossil fuel-derived CO_2 but is also sensitive to land and ocean carbon cycling and uptake. Using updated records, we show that no plausible combination of sources and sinks of CO_2 from fossil fuel, land, and oceans can explain the observed ^{13}C-Suess effect unless an increase has occurred in the $^{13}C/^{12}C$ isotopic discrimination of land photosynthesis. A trend toward greater discrimination under higher CO_2 levels is broadly consistent with tree ring studies over the past century, with field and chamber experiments, and with geological records of C_3 plants at times of altered atmospheric CO_2, but increasing discrimination has not previously been included in studies of long-term atmospheric $^{13}C/^{12}C$ measurements. We further show that the inferred discrimination increase of $0.014 \pm 0.007‰$ ppm^{-1} is largely explained by photorespiratory and mesophyll effects. This result implies that, at the global scale, land plants have regulated their stomatal conductance so as to allow the CO_2 partial pressure within stomatal cavities and their intrinsic water use efficiency to increase in nearly constant proportion to the rise in atmospheric CO_2 concentration.

carbon cycle | photosynthesis | isotope | water use efficiency | carbon-13 Suess effect

The accumulation of excess CO_2 in the atmosphere over the past century has been associated with a closely related decrease in the $^{13}C/^{12}C$ ratio of the CO_2. This isotopic trend, first reported in 1979 (1), has become known as the "carbon-13 Suess effect" (2), by analogy to the decrease in the radiocarbon (^{14}C) content of CO_2 discovered in 1955 by Hans Suess (3). Measurements from air trapped in ice cores (4) show that the preindustrial background $\delta^{13}C$ value was around $-6.4‰$. As of 2014, the average value was around $-8.4‰$ (Figs. 1 and 2).

The ^{13}C-Suess effect, like that for ^{14}C, is driven primarily by the input of CO_2 from fossil fuels. Fossil fuels are slightly depleted in ^{13}C because they were initially formed from photosynthesis, which involves isotopic discrimination, that is, selective uptake of $^{12}CO_2$ over $^{13}CO_2$. The emission of fossil fuel CO_2 therefore lowers the atmospheric $^{13}C/^{12}C$ ratio. A second important influence on the ^{13}C-Suess effect is the natural back-and-forth exchanges of CO_2 with land and ocean carbon reservoirs. These gross exchanges, also known as "disequilibrium fluxes," scramble carbon atoms between reservoirs, thereby spreading the Suess effect into the land and oceans while reducing the atmospheric signal. A third influence is net gain or loss of carbon by the land biosphere, which is depleted in ^{13}C because of photosynthesis, similar to fossil fuels. A sink for excess CO_2 on land therefore offsets the influence of fossil fuel burning, not just on CO_2 amount, but also on its isotopic composition. In contrast, ocean uptake of excess CO_2 has little influence on $\delta^{13}C$ of atmospheric CO_2 (5).

The ^{13}C-Suess effect has been applied to quantify the global land carbon sink and hence the ocean sink by mass balance of total CO_2 (6–8). The method resolves the land sink from the observed $\delta^{13}C$ trend after correcting for the fossil fuel and disequilibrium flux contributions. The method is not without challenges, however. The isotopic discrimination of photosynthesis can vary, depending on photosynthetic pathway (e.g., C_3 vs. C_4) and the leaf environment (e.g., water stress). Systematic variations in discrimination, in turn, can impart variability in the disequilibrium fluxes, which are hard to quantify. For example, during El Nino events, drought in tropical land masses not only causes a temporary release of CO_2, but also reduces discrimination, causing variations in $\delta^{13}C$ of CO_2 that are not related to this CO_2 source (9–13) and that are not represented in traditional disequilibrium flux estimates (6, 14–16). A further difficulty is that the global $\delta^{13}C$ budget does not balance convincingly (11).

Here, we update the longest direct time series for $\delta^{13}C$ of CO_2, starting in 1978, from the flask program at the Scripps Institution of Oceanography. Rather than resolving carbon sinks, we use data/model comparison to show that there must exist an additional process, previously neglected, that reduces the atmospheric ^{13}C-Suess effect. We suggest that the missing process is an ongoing systematic global increase in the isotopic discrimination of land photosynthesis, which has implications for trends in plant water-use efficiency at the global scale.

We derive a global record by combining data from Mauna Loa and South Pole after removing seasonal cycles. We interpret the

Significance

Climate change and rising CO_2 are altering the behavior of land plants in ways that influence how much biomass they produce relative to how much water they need for growth. This study shows that it is possible to detect changes occurring in plants using long-term measurements of the isotopic composition of atmospheric CO_2. These measurements imply that plants have globally increased their water use efficiency at the leaf level in proportion to the rise in atmospheric CO_2 over the past few decades. While the full implications remain to be explored, the results help to quantify the extent to which the biosphere has become less constrained by water stress globally.

Author contributions: R.F.K. and H.D.G. designed research; R.F.K., H.D.G., L.R., and S.C.P. performed research; H.D.G., L.R., S.C.P., A.B., and H.A.J.M. contributed new reagents/analytic tools; R.F.K., H.D.G., L.R.W., L.R., and S.C.P. analyzed data; R.F.K., H.D.G., L.R.W., L.R., J.B., S.C.P., Y.S., and H.A.J.M. wrote the paper; and Y.S. performed supporting calculations.

The authors declare no conflict of interest.

This article is a PNAS Direct Submission.

Data deposition: The original data reported in this paper have been deposited at scrippsCO2.ucsd.edu.

[1]To whom correspondence should be addressed. Email: rkeeling@ucsd.edu.

This article contains supporting information online at www.pnas.org/lookup/suppl/doi:10.1073/pnas.1619240114/-/DCSupplemental.

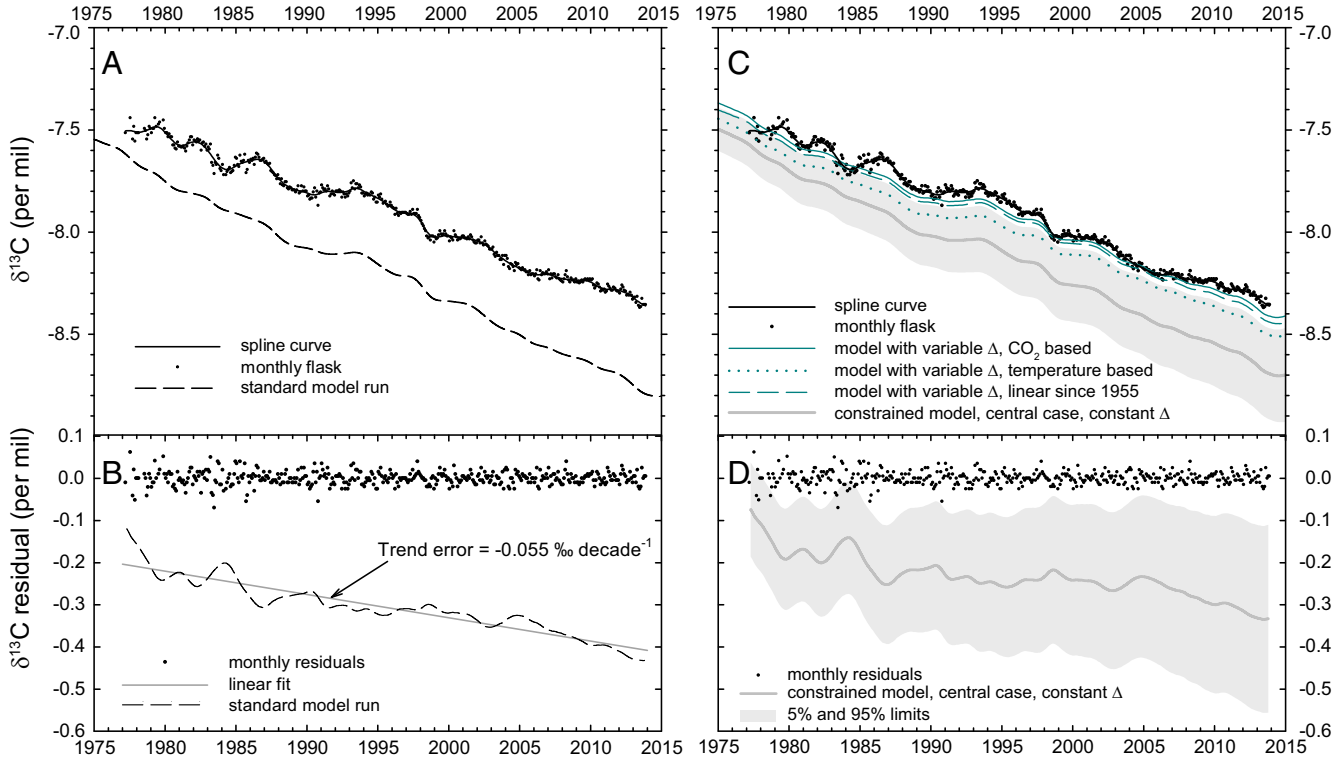

Fig. 1. Measured and modeled trends in $\delta^{13}C$ of atmospheric CO_2. Measurements are based on average monthly values at Mauna Loa and South Pole stations, after removing seasonal cycles. (*A*) Measurements vs. standard model run. (*B*) Measurements and standard model run as residuals from spline fit. The linear fit through the model residual with slope of –0.055‰ decade^{-1} quantifies the failure of the standard model to account for the observed $\delta^{13}C$ trend. This slope error is independent of the overall offset of the model from the data, which depends on the assumed preindustrial model value of –6.4‰. (*C* and *D*) Measurements vs. optimized model run, where the optimization is based on radiocarbon and other constraints, also allowing for ocean warming and wind shift effects (*SI Appendix*). Gray shading reflects 5% and 95% confidence limits on optimized run. Also shown are runs for three scenarios with variable land discrimination Δ, each of which was optimized to also match the rate of change in $\delta^{13}C$ since 1978. All model runs initiated at a value of $\delta^{13}C$ = –6.4‰ in year 1765.

trend using a model (*Materials and Methods* and *SI Appendix*), run from 1765 to 2015, which treats the atmosphere and the ocean mixed layer as well-mixed reservoirs, the land biosphere as consisting of three boxes, and the ocean interior as a 1D diffusive system. The model, which is constrained by radiocarbon measurements, includes a one-box representation of the marine biological pump and allows for ocean warming (17, 18) and the warming-associated impact on CO_2 solubility and air–sea isotopic fractionation. Interannual variations in globally averaged sea surface temperature were also included as were effects of interannually varying winds over the ocean. The model is run as a single deconvolution, that is, the land sink is adjusted to balance the global carbon budget. The trend in atmospheric $\delta^{13}C$ is diagnosed from the simulated carbon fluxes under different assumptions for land discrimination, and these results are then compared with $\delta^{13}C$ observations.

Results

The standard model run, which holds land discrimination constant at 18‰ (detailed in *SI Appendix*, Table S1), is compared with observations in Fig. 1*A*. This run yields a $\delta^{13}C$ trend that has an offset from the observations that grows with time. We focus here on the trend in offset, noting the average offset is sensitive to uncertainty in the ice core-based preindustrial $\delta^{13}C$ value (−6.4‰ in 1765) and laboratory-to-laboratory calibration offsets. The trend in offset reflects the tendency of the model to overpredict the decrease in atmospheric $\delta^{13}C$ from 1978 to 2014. This overprediction is much larger than the uncertainty in the $\delta^{13}C$ data and well resolved despite interannual variability in the observations. The model also underrepresents interannual variability in part because no climatic impacts on discrimination are included (9, 11, 12). A linear fit to the model–data difference (Fig. 1*B*) yields a trend error of –0.055 ± 0.013‰ decade^{-1} or –0.20 ± 0.05‰ over the whole 36-y-long record, where the uncertainty accounts for measurement imprecision and serial correlation associated with interannual variability in the model–data difference, but not systematic model error (*SI Appendix*, section 5).

To investigate the robustness of the model and possible sources of model–data trend differences, we carry out multiple runs that span a wide range of model parameters (*SI Appendix*, Tables S2 and S4). The parameter which most strongly influences the land and ocean CO_2 sinks is the ocean vertical diffusivity, but this parameter only weakly influences the atmospheric $\delta^{13}C$ trend (*SI Appendix*, Fig. S3). The parameters with the greatest influence are the coefficients governing air–sea exchange and the turnover of carbon in the land biosphere. The collective impact of these and several other parameters including total fossil fuel emissions and the land photosynthetic fertilization factor (*SI Appendix*, Table S2, set 1) on modeled ^{13}C-Suess effect is quite effectively constrained by requiring the model to also match estimates for the total ^{14}C produced from nuclear weapons testing and the associated ocean ^{14}C excess (19, 20) (*SI Appendix*, Figs. S4 and S5). Applying these ^{14}C constraints shows that the parameters in the standard model are nearly optimal, while also quantifying uncertainties.

Another important influence is ocean warming, which reduces air–sea equilibrium fractionation and increases the ocean disequilibrium flux. This drives atmospheric $\delta^{13}C$ upward, reducing the model/data trend mismatch (*SI Appendix*, Table S2, set 2). Accounting for this warming reduces the overprediction of the

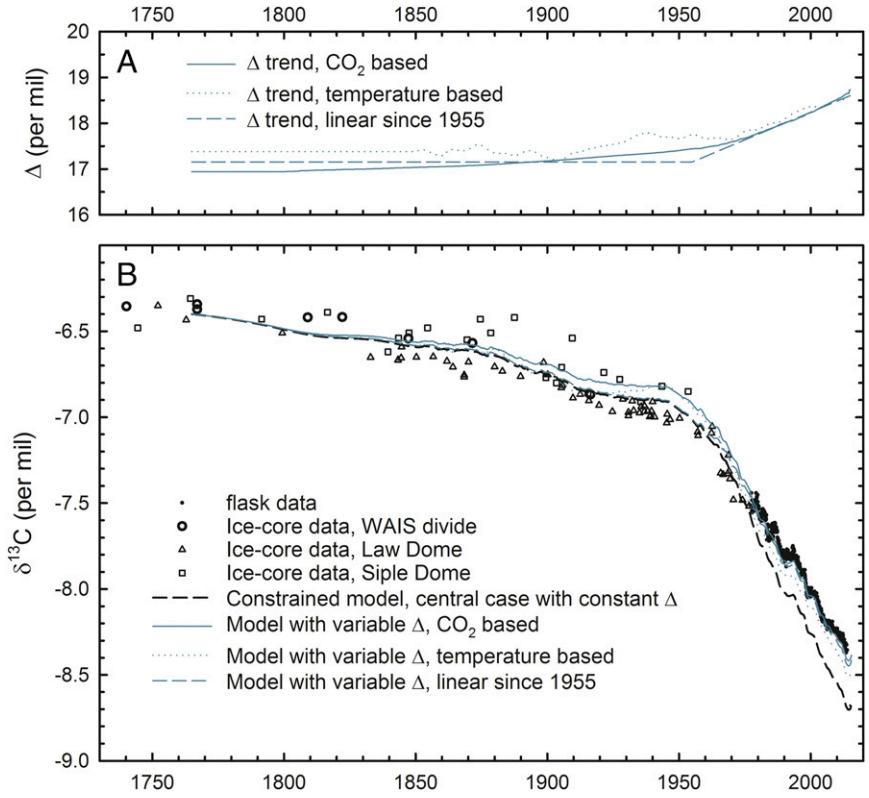

Fig. 2. (*A*) Variation in the isotopic discrimination of land photosynthesis for three variable Δ scenarios, each of which was optimized to match the rate of change in $\delta^{13}C$ since 1978. (*B*) Measured vs. modeled $\delta^{13}C$. Ice core data sources: WAIS divide (4), Law Dome (53), and Siple Station (54). All runs initiated at a value of $\delta^{13}C = -6.4‰$ in year 1765. In the model–data comparison, trends are significant but not absolute differences.

trend from $-0.055‰$ decade^{-1} to $-0.035‰$ decade^{-1}. Potentially countering this warming effect, however, are shifts in the surface winds governing air–sea gas exchange. Over recent decades, the surface winds at high latitudes have generally strengthened (21), thereby increasing the gas exchange rate in colder regions, which by itself could cause a cooling trend in the gas exchange-weighted sea surface temperature, thereby countering the overall ocean-warming effect. We quantify this wind shift effect (*SI Appendix*, Table S2, set 3), using three different global wind speed products and two different assumptions for the dependence of gas exchange on winds (linear vs. quadratic). Overall, the wind shift effect contributes uncertainty to the modeling, while generally increasing the modeled trend error.

We also explore a wide range of additional processes with apparently minor impacts on the $\delta^{13}C$ trend. We find that inclusion of a steady marine biological pump in the ocean model has very little impact. Allowing for increases in marine pump efficiency with time, as might occur due to warming-induced stratification (22), slightly increases the overprediction error (*SI Appendix*, Table S2, set 4). The trend error is slightly reduced ($-0.052‰$ decade^{-1} instead of $-0.055‰$ decade^{-1}) by allowing for a secular increase in the isotopic discrimination of marine photosynthesis (23) owing to rising CO_2 (*SI Appendix*, Table S2, set 5). We also explore the impact of uncertainty in $\delta^{13}C$ of fossil fuel emissions (*SI Appendix*, Table S2, set 6) and the uncertainty in the (assumed constant) value of land discrimination (*SI Appendix*, Table S2, set 7). However, taking these effects into account, including uncertainty in the standard model parameters (as constrained by radiocarbon) and the warming/wind effects, it still does not appear possible to account for the observed trend ($P < 0.020$) (Fig. 1 *C* and *D*, and *SI Appendix*, Fig. S6).

We identify only one reasonable way to adjust the model to match the atmospheric $\delta^{13}C$ trend, which is to assume that land discrimination has increased systematically over time. A variant of the central constrained model run, which assumes that discrimination has increased linearly with CO_2 concentration is shown in Fig. 1*C*. This run was optimized to match the observed $\delta^{13}C$ trend by adjusting the sensitivity of discrimination to CO_2. For this run, a sensitivity of $0.014‰$ ppm^{-1} was required, although this run, by itself, does not explore the full uncertainties. Using a large ensemble of runs in model parameters and input datasets (*SI Appendix*, section 5) and imposing constraints based on radiocarbon and other estimated parameter uncertainties, and adjusting the discrimination changes to match the observed trend from 1978 to 2014 to within the uncertainties, we find an optimum sensitivity of $0.014 \pm 0.007‰$ ppm^{-1}.

It is equally possible to match the observed $\delta^{13}C$ trend by assuming that discrimination has increased for other reasons, unrelated to the rise in CO_2. We therefore investigated two additional scenario types, either assuming the discrimination changed linearly in proportion to changes in global average surface air temperature since 1850 or second assuming discrimination was constant from 1765 to 1955, after which it increased linearly with time for an unspecified reason. Variants of the standard run which allow for changing discrimination according to these scenarios and which are optimized to match the observed trend are also shown in Fig. 1*C*. To quantify uncertainties, we explored an ensemble of runs that considered all three discrimination change scenarios (CO_2 based, temperature based, linear; *SI Appendix*, section 5). We use this ensemble to place constraints on the discrimination changes from 1975 to 2005, which is well constrained by the data because of the several-year lag between discrimination changes and the atmospheric response. Accordingly, we find that a discrimination increase of $0.66 \pm 0.34‰$ (90% CI from 0.18 to $1.2‰$) is required from 1975 to 2005 to match the observed $\delta^{13}C$ trend to within the

uncertainties. Over this period, atmospheric CO_2 increased from 330 to 377 ppm. Dividing the discrimination increase of 0.65 ± 0.33‰ by the 47-ppm CO_2 increase, again supports a sensitivity estimate of 0.014 ± 0.007‰ ppm^{-1}. We find that the runs with changing discrimination that are constrained to match the trend from 1978 to 2014 also agree, to within the larger uncertainties, with the ice core data from 1765 to 1978, as shown in Fig. 2.

Discussion

Increasing land discrimination reduces the atmospheric ^{13}C-Suess effect by increasing the accumulation of ^{12}C over ^{13}C in the land biosphere, thus also yielding an amplified Suess effect in the land biosphere. An effect of this sort is indeed generally corroborated by tree ring $\delta^{13}C$ sequences, which show decreases in $\delta^{13}C$ that are stronger than the observed atmospheric trend, depending on location and vegetation type (23–26). The stronger decrease in tree rings is commonly assumed to result from the impact of rising CO_2 on discrimination, and corrections between 0.0 and 0.02‰ ppm^{-1} are typically applied to tree ring $\delta^{13}C$ sequences to recover signals related to other phenomena besides rising CO_2 (24, 25). Our global estimate of 0.014‰ ppm^{-1} falls within this range.

Evidence for increasing discrimination with higher CO_2 has also been found in chamber and field studies on C_3 plants under altered CO_2 conditions as well as from paleo data (26, 27), although exceptions to this pattern have also been found (28). In a compilation of prior work, Schubert and Jahren (26) find a best-fit sensitivity of ∼0.014‰ ppm^{-1} at 355 ppm, which also matches well with the sensitivity we require to match the atmospheric $\delta^{13}C$ trend.

The atmospheric $\delta^{13}C$ data thus provide strong evidence that land discrimination is increasing on a global scale. This shift must largely reflect changes in C_3 plants, which produce 95% of global biomass (29) and therefore control the disequilibrium flux that is tied to changing discrimination on decadal and longer timescales. This shift has implications for understanding leaf-level processes that impact growth and water balance of global ecosystems.

In C_3 plants, discrimination is related to the ratio of the CO_2 concentration within the stomatal cavity (C_i) to the ambient CO_2 concentration (C_a) via the following:

$$\Delta = a + (b-a)(C_i/C_a) - (b-a_m)(A/C_a)/g_i - f\Gamma^*/C_a, \qquad [1]$$

where a = 4.4‰, b = 30‰, a_m = 1.8‰, A is leaf-level gross photosynthesis, g_i is mesophyll conductance, f is the discrimination due to photorespiration, and Γ^* is the CO_2 compensation point in the absence of day respiration (30–32). The last two terms in Eq. **1** account for mesophyll and photorespiration effects, which are typically neglected but are relevant for a first-order understanding of how Δ varies with C_a (32). If these terms can be quantified, then changes in Δ can be related to changes in C_i/C_a, which in turn constrains the stomatal conductance influencing both CO_2 gain and water loss. The constraint can be framed in terms of the leaf-level intrinsic water use efficiency, which measures photosynthesis per unit stomatal conductance and is given by the following:

$$\text{iWUE} = A/g_s = C_a(1 - C_i/C_a)/1.6, \qquad [2]$$

where g_s is the stomatal conductance and 1.6 is the ratio of the diffusivities of H_2O and CO_2 in air (33).

The mesophyll and photorespiration terms in Eq. **1** are both negative, but their absolute magnitudes decrease with C_a owing to the presence of C_a in the denominator. These terms therefore both contribute to increasing discrimination with rising CO_2. For a change in C_a from 330 to 377 ppm, the photorespiration term in Eq. **1** increases discrimination by 0.19 ± 0.06‰, contributing to a sensitivity of 0.0041 ± 0.0014‰ ppm^{-1}. This estimate adopts f = 12 ± 4‰ (31) and $\Gamma^* \approx$ 43 ppm, appropriate for leaves at a typical temperature of 25 °C (34). The mesophyll term is potentially quite variable, as it depends on A and g_i, which vary with leaf environment and plant type (35). Also, A generally increases with C_a, but slower than proportionally (36), thus partly offsetting the impact of C_a in the denominator. Allowing that A has increased linearly with CO_2 at a rate corresponding to a 45 ± 25% increase for a doubling in C_a (36) and taking representative values (32) (A = 9 ± 3 μmol·m^{-2}·s^{-1}; g_i = 0.2 ± 0.05 mol·m^{-2}·s^{-1}), we estimate a globally averaged mesophyll contribution to the sensitivity (centered on ∼355 ppm) of 0.006 ± 0.003‰ ppm^{-1}. Added together, the mesophyll and photorespiration terms thus contribute 0.010 ± 0.004‰ ppm^{-1} to the overall sensitivity.

This calculation shows that mesophyll and photorespiration terms in Eq. **1** are potentially sufficient to account the full global sensitivity of 0.014 ± 0.007‰ ppm^{-1} estimated from the ^{13}C budget to within the uncertainties. It follows from Eq. **1** that C_i/C_a has remained constant to within the uncertainties, and from Eq. **2** that iWUE has increased in proportion to C_a to within the uncertainties. We estimate a residual sensitivity after correcting for mesophyll and photorespiration effects of 0.004 ± 0.008‰ ppm^{-1}. Assuming this near-zero residual sensitivity holds over the 20th century when C_a increased by 71 ppm (from 296 to 367 ppm), this corresponds to a residual change in Δ of 0.3 ± 0.6‰. From this, we calculate from the second term on the right-hand side of Eq. **1**, a change in C_i/C_a of 0.011 ± 0.022 or 1.5 ± 3.3% (relative to a mean value of C_i/C_a ∼0.7 for C_3 photosynthesis). This corresponds to a relative increase in iWUE of 20 ± 9% over the 20th century, driven primarily by the additional factor of C_a that appears in Eq. **2**.

Our estimate of the global iWUE change of 20 ± 9% for the 20th century can be compared with results for Europe based on tree ring $\delta^{13}C$ sequences by Frank et al. (37). However, because Frank et al. (37) neglected the mesophyll and photorespiration terms in Eq. **1**, we first add 14 ± 10% to their estimates of relative changes in iWUE for these effects, yielding increase in iWUE of 28 ± 14% for broadleaf and 36 ± 11% for conifer sites. Here, we assessed the mesophyll/photorespiration correction by carrying out calculations with and without these terms in Eq. **1** and also using b = 27‰ for the uncorrected calculation, as assumed by Frank et al. (37). Assuming these European estimates are representative of the global extratropics, the comparison with our global estimate implies that tropical ecosystems, which must exert considerable leverage on the long-term $\delta^{13}C$ trend, have also potentially seen increases in iWUE. Our results stand in contrast with results from direct water vapor and CO_2 flux measurements of North American forests from the early 1990s through 2010 (38), which appeared to show C_i remaining essentially constant with time, therefore requiring even larger increases in iWUE. The time period covered by direct flux measurements may be too short, however, to resolve systematic trends that are evident globally over the longer time frame of the atmospheric and tree ring $\delta^{13}C$ measurements.

A possible explanation for near constancy in the ratio C_i/C_a is provided by the optimality hypothesis, which assumes that plants adjust their stomatal conductance to maximize overall carbon gain, considering also the metabolic costs of supplying water for transpiration (39–41). This hypothesis predicts that C_i/C_a will vary in association with plant traits, including sapwood-to-leaf area ratios, as well as on the leaf-to-air vapor pressure deficit and ambient temperature, which influences water viscosity. However, C_i/C_a is otherwise predicted to be largely independent of ambient of C_a and should therefore remain roughly constant as atmospheric CO_2 rises, at least over intermediate ranges (42). Optimal stomatal behavior must break down at sufficiently high C_a because stomatal and cuticle resistance must have upper bounds. In this high limit, $C_a - C_i$ presumably approaches a constant and C_i/C_a approaches unity, consistent with observations at very high CO_2 where $\Delta \approx b$ (43).

Our study also has implications for using $\delta^{13}C$ data to constrain the land/ocean partitioning of the global CO_2 sinks, highlighting a problem with previous applications that decouple the ocean CO_2 sink from the ocean $\delta^{13}C$ disequilibrium flux. As mentioned above, the main parameter which influences the sink partitioning is the ocean vertical diffusivity, but this parameter has little impact on the predicted atmospheric $\delta^{13}C$ trend. This insensitivity was noted in early work (2) but neglected in most subsequent studies (11, 16, 44). The insensitivity arises because of compensation between two terms in the isotopic budget, that is, the ocean disequilibrium and land sink terms (*SI Appendix*, Fig. S3). The ocean disequilibrium flux depends on ocean diffusivity directly, via the impact of vertical mixing on the uptake of the $\delta^{13}C$ isotopic signal by the oceans. The land sink and its effect on $\delta^{13}C$ depend on diffusivity indirectly, via its control of the ocean sink and hence the land sink via global CO_2 mass balance. The two effects tend to cancel in terms of the impact on the atmospheric $\delta^{13}C$ trend. Because of this compensation, the atmospheric $\delta^{13}C$ trend does not provide a useful constraint on global land/ocean sink partitioning. Instead, it provides a constraint on the sum of land and ocean sinks which is redundant to the constraint from the atmospheric CO_2 trend. Previous studies have overcome this limitation mainly by relying on measurements of $\delta^{13}C$ in the ocean (7, 11, 44). This approach, however, neglects the fact that the ocean CO_2 sink and the ocean disequilibrium flux are not mechanistically independent, as they both depend on the rate of vertical mixing or diffusion in the ocean. An additional need would be to show that the ocean sink and disequilibrium fluxes are mutually compatible, given this link.

The 1D ocean model used here has the advantage that it maintains a mechanistic link between total CO_2 and ^{13}C in the ocean. On the other hand, this very simple model cannot fully capture complexities in the coupling between total CO_2 and isotopic air–sea exchanges, and further studies with 3D ocean models are clearly warranted. In any case, the land–ocean sink partitioning is now quite well constrained, not just by radiocarbon measurements, but also by measurements of atmospheric O_2 (45) and of additional ocean tracers (46), which all give convergent estimates. These advances allow the ^{13}C budgeting to be turned around, from constraining sinks to constraining discrimination effects.

Campbell et al. (47) recently reported a 20th-century increase in land gross primary production (GPP) of 31 ± 5% based on trends in atmospheric carbonyl sulfide (OCS). GPP can related to iWUE according to the following:

$$\mathrm{GPP} = \mathrm{iWUE} \cdot \mathrm{Tr}/\mathrm{VPD}, \qquad [3]$$

where Tr is leaf transpiration (in moles of H_2O per year) and VPD is an average measure of leaf-to-air vapor pressure deficit (in pascals). Together, the global trends in GPP (from OCS) and iWUE (from $\delta^{13}C$) require that Tr/VPD has increased globally by 11 ± 10% over the 20th century. At the leaf level, Tr/VPD is equivalent to stomatal conductance, which is expected to have decreased under elevated CO_2 (48), but this could be offset globally by increased leaf area and growing season length (37). Eq. **3** provides an alternate framework using iWUE for estimating trends in GPP, once reliable estimates of trends in Tr and VPD are developed.

Despite the low contribution of C_4 photosynthesis to global biomass, a reviewer raised the concern that shifts between C_3 and C_4 photosynthesis might significantly impact the long-term atmospheric $\delta^{13}C$ trend, especially via the C_4 contribution to soil carbon. In this context, Scholze et al. (10) showed that C_3/C_4 changes have caused global average Δ (NPP-weighted) to decrease by ∼0.5‰ since preindustrial times, dominated by land use via conversion of forest to C_4 pasture before 1960, with only minor C_3/C_4 effects from climate and CO_2 fertilization. To address this effect, we imposed the land use-driven C_3/C_4 discrimination change as an additional time-varying forcing on our model and found that this drives an overall decrease in atmospheric $\delta^{13}C$ of ∼0.1‰ from 1765 to 1975, with a weak recovery of ∼0.01‰ since 1975. Allowing for this effect decreases the model–data trend error (Fig. 1*B*) very slightly by ∼0.002‰ decade^{-1}, requiring a very small decrease in the discrimination sensitivity to CO_2 (from 0.014 to 0.013‰ ppm^{-1}) to match the observed trend since 1978. This is likely an upper bound to any C_3/C_4 effect, because it neglects the shorter turnover time of C_4 compared with C_3 carbon, both in plant tissues as well as in soil carbon (49). Earlier studies suggesting larger C_3/C_4 effects appear to have assumed unrealistically long turnover of soil carbon (10, 50). On this basis, the shift in Δ required by the recent atmospheric budget indeed appears to be heavily dominated by C_3 photosynthesis and not by C_3/C_4 shifts.

During review, we also learned of recent study using tree ring isotopic data (51), mainly from Europe, boreal Asia, and western North America, which found no systematic change in Δ through the 20th century, contrary to our atmospheric results and contrary to other tree ring studies (24, 25) which suggest Δ has increased. A direct comparison is difficult, however, because of differences in spatial coverage, with the atmospheric data giving a more truly global constraint over recent decades. The recent tree ring study (51) implies a 20th-century increase in iWUE of 27% compared with our atmospheric estimate of 20% globally, but the comparison is complicated by inconsistent treatment of the photorespiration and mesophyll terms in Eq. **1**.

Our analysis yields a balanced global $\delta^{13}C$ budget (*SI Appendix*, Table S5) that is backed by radiocarbon measurements in the atmosphere and oceans and consistent with a mechanistic understanding of the controls on terrestrial isotopic discrimination. Recognizing the insensitivity of the $\delta^{13}C$ trend to the land/ocean sink partitioning and other advances in carbon budgeting, our study involves a change in perspective on the main application of measuring the long-term $\delta^{13}C$ trend, from resolving sinks to resolving changes in discrimination.

Materials and Methods

Atmospheric samples were collected in 5-L flasks and analyzed at Scripps and Groningen using methods described in Keeling et al. (52) and *SI Appendix*. Based on short-term variability in monthly mean $\delta^{13}C$ values at the sampling sites and based on limitations to long-term calibration, we allow an uncertainty in the long-term trend in $\delta^{13}C$ of ±0.01‰ decade^{-1} over the ∼36-y time frame of the measurements, not counting the additional error due to serial correlation from interannual variability. Model calculations were carried out using a variant of the box diffusion model as described briefly in the Introduction and detailed in *SI Appendix*. The model was forced with historical estimates of CO_2 emissions from fossil fuel burning, land use change, changing sea surface temperature, changing wind impact on air–sea gas exchange, including a depiction of the marine biological pump, and allowing for changes in land and ocean photosynthetic discrimination. Three types of scenarios for changing land discrimination were investigated, as described previously. The scenario for changing marine discrimination is based on Young et al. (23). The model was run from year 1765 to 2015. A total of 2,760 runs were carried out to explore the impact of uncertainty in model parameters and input datasets in the context of two questions: (*i*) What is the probability distribution of the modeled atmospheric $\delta^{13}C$ trend, considering the full range of uncertainty but keeping land biospheric discrimination constant ? (*ii*) What is the probability distribution of the long-term trend in land biospheric discrimination that is consistent with the observed $\delta^{13}C$ trend and other constraints. For both questions, the model runs were weighted according to their ability to account for the estimated total bomb radiocarbon production and ocean radiocarbon excess in year 1994. For the second question, the runs were also weighted according to their ability to account for the observed long-term trend in atmospheric $\delta^{13}C$ trend from 1978 to 2014 to within the uncertainties.

ACKNOWLEDGMENTS. We thank Graham Farquhar and an anonymous reviewer for very helpful comments. This work was largely motivated by conversations between R.F.K. and Dr. Robert Bacastow, who had deep insight into the controls on $\delta^{13}C$ variations. We thank Marko Scholze for providing time series of global discrimination related to C_3/C_4 conversion. The CO_2 and $\delta^{13}C$ measurements were also supported by National Oceanic and Atmospheric Administration (NOAA) staff at the Mauna Loa and South Pole Observatories for the collection of air samples. This work was supported by the

US NSF, the Department of Energy (DOE), and National Aeronautics and Space Administration (NASA) under Grants 1304270, DE-SC0012167, and NNX17AE74G, and by the Eric and Wendy Schmidt Fund for Strategic Innovation.

Any opinions, findings, and conclusions or recommendations expressed in this material are those of the authors and do not necessarily reflect the views of NOAA, NSF, DOE, or NASA.

1. Keeling CD, Mook WG, Tans PP (1979) Recent trends in the $^{13}C/^{12}C$ ratio of atmospheric carbon dioxide. *Nature* 277:121–123.
2. Keeling CD (1979) The Suess effect: ^{13}Carbon-^{14}Carbon interrelations. *Environ Int* 2: 229–300.
3. Suess HE (1955) Radiocarbon concentration in modern wood. *Science* 122:415–417.
4. Bauska TK, et al. (2015) Links between atmospheric carbon dioxide, the land carbon reservoir and climate over the past millennium. *Nat Geosci* 8:383–387.
5. Tans PP, Berry JA, Keeling RF (1993) Oceanic $^{13}C/^{12}C$ observations: A new window on ocean CO_2 uptake. *Global Biogeochem Cycles* 7:353–368.
6. Keeling CD, Whorf TP, Wahlen M, Vanderplicht J (1995) Interannual extremes in the rate of rise of atmospheric carbon-dioxide since 1980. *Nature* 375:666–670.
7. Quay PD, Tilbrook B, Wong CS (1992) Oceanic uptake of fossil-fuel CO_2: Carbon-13 evidence. *Science* 256:74–79.
8. Trudinger C, Enting I, Etheridge D, Francey R, Rayner P (2005) The carbon cycle over the past 1000 years inferred from the inversion of ice core data. *A History of Atmospheric CO2 and Its Effects on Plants, Animals, and Ecosystems*, eds Ehleringer JR, Cerling TE, Dearing MD (Springer, New York), pp 329–349.
9. Randerson JT, et al. (2002) A possible global covariance between terrestrial gross primary production and C-13 discrimination: Consequences for the atmospheric C-13 budget and its response to ENSO. *Global Biogeochem Cycles* 16:83-1–83-16.
10. Scholze M, Ciais P, Heimann M (2008) Modeling terrestrial C-13 cycling: Climate, land use and fire. *Global Biogeochem Cycles* 22:GB1009.
11. van der Velde I, et al. (2013) Biosphere model simulations of interannual variability in terrestrial $^{13}C/^{12}C$ exchange. *Global Biogeochem Cycles* 27:637–649.
12. Alden CB, Miller JB, White JW (2010) Can bottom-up ocean CO_2 fluxes be reconciled with atmospheric ^{13}C observations? *Tellus B Chem Phys Meterol* 62:369–388.
13. Miller JB, Tans PP, White JW, Conway TJ, Vaughn BW (2003) The atmospheric signal of terrestrial carbon isotopic discrimination and its implication for partitioning carbon fluxes. *Tellus B Chem Phys Meterol* 55:197–206.
14. Enting I, Trudinger C, Francey R (1995) A synthesis inversion of the concentration and $\delta^{13}C$ of atmospheric CO_2. *Tellus B Chem Phys Meterol* 47:35–52.
15. Keeling CD, et al. (1989) A three-dimensional model of atmospheric CO_2 transport based on observed winds: 1. Analysis of observational data. *Aspects of Climate Variability in the Pacific and Western Americas, Geophysical Monograph Series*, ed Peterson DH (American Geophysical Union, Washington, DC), Vol 55, pp 165–236.
16. Francey RJ, et al. (1995) Changes in oceanic and terrestrial carbon uptake since 1982. *Nature* 373:326–330.
17. Kennedy J, Rayner N, Smith R, Parker D, Saunby M (2011) Reassessing biases and other uncertainties in sea surface temperature observations measured in situ since 1850: 1. Measurement and sampling uncertainties. *J Geophys Res Atmos* 116:D14103.
18. Kennedy J, Rayner N, Smith R, Parker D, Saunby M (2011) Reassessing biases and other uncertainties in sea surface temperature observations measured in situ since 1850: 2. Biases and homogenization. *J Geophys Res Atmos* 116:D14104.
19. Naegler T, Levin I (2006) Closing the global radiocarbon budget 1945–2005. *J Geophys Res* 111:D12311.
20. Naegler T (2009) Reconciliation of excess ^{14}C-constrained global CO_2 piston velocity estimates. *Tellus B Chem Phys Meterol* 61:372–384.
21. Young IR, Zieger S, Babanin AV (2011) Global trends in wind speed and wave height. *Science* 332:451–455.
22. Sarmiento JL, Hughes TMC, Stouffer RJ, Manabe S (1998) Simulated response of the ocean carbon cycle to anthropogenic climate warming. *Nature* 393:245–249.
23. Young JN, Bruggeman J, Rickaby REM, Erez J, Conte M (2013) Evidence for changes in carbon isotopic fractionation by phytoplankton between 1960 and 2010. *Global Biogeochem Cycles* 27:505–515.
24. Treydte KS, et al. (2009) Impact of climate and CO_2 on a millennium-long tree-ring carbon isotope record. *Geochim Cosmochim Acta* 73:4635–4647.
25. McCarroll D, et al. (2009) Correction of tree ring stable carbon isotope chronologies for changes in the carbon dioxide content of the atmosphere. *Geochim Cosmochim Acta* 73:1539–1547.
26. Schubert BA, Jahren AH (2015) Global increase in plant carbon isotope fractionation following the Last Glacial Maximum caused by increase in atmospheric pCO_2. *Geology* 43:435–438.
27. Schubert BA, Hope Jahren A (2013) Reconciliation of marine and terrestrial carbon isotope excursions based on changing atmospheric CO_2 levels. *Nat Commun* 4:1653.
28. Battipaglia G, et al. (2013) Elevated CO_2 increases tree-level intrinsic water use efficiency: Insights from carbon and oxygen isotope analyses in tree rings across three forest FACE sites. *New Phytol* 197:544–554.
29. Still CJ, Berry JA, Collatz GJ, DeFries RS (2003) Global distribution of C3 and C4 vegetation: Carbon cycle implications. *Global Biogeochem Cycles* 17:6-1–6-14.
30. Farquhar GD, Oleary MH, Berry JA (1982) On the relationship between carbon isotope discrimination and the inter-cellular carbon-dioxide concentration in leaves. *Aust J Plant Physiol* 9:121–137.
31. Cernusak LA, et al. (2013) Environmental and physiological determinants of carbon isotope discrimination in terrestrial plants. *New Phytol* 200:950–965.
32. Seibt U, Rajabi A, Griffiths H, Berry JA (2008) Carbon isotopes and water use efficiency: Sense and sensitivity. *Oecologia* 155:441–454.
33. Ehleringer JR, Hall AE, Farquhar GD (1993) *Stable Isotopes and Plant-Water Relationships* (Academic, New York).
34. Bonan GB, et al. (2011) Improving canopy processes in the Community Land Model version 4 (CLM4) using global flux fields empirically inferred from FLUXNET data. *J Geophys Res Biogeosci* 116:G02014.
35. Sun Y, et al. (2014) Impact of mesophyll diffusion on estimated global land CO_2 fertilization. *Proc Natl Acad Sci USA* 111:15774–15779.
36. Franks PJ, et al. (2013) Sensitivity of plants to changing atmospheric CO_2 concentration: From the geological past to the next century. *New Phytol* 197:1077–1094.
37. Frank D, et al. (2015) Water-use efficiency and transpiration across European forests during the Anthropocene. *Nat Clim Chang* 5:579–583.
38. Keenan TF, et al. (2013) Increase in forest water-use efficiency as atmospheric carbon dioxide concentrations rise. *Nature* 499:324–327.
39. Cowan I, Farquhar G (1977) Stomatal function in relation to leaf metabolism and environment. *Integration of Activity in the Higher Plant*, ed Jennings DH (Cambridge Univ Press, Cambridge, UK), pp 471–505.
40. Medlyn BE, et al. (2011) Reconciling the optimal and empirical approaches to modelling stomatal conductance. *Glob Change Biol* 17:2134–2144.
41. Prentice IC, Dong N, Gleason SM, Maire V, Wright IJ (2014) Balancing the costs of carbon gain and water transport: Testing a new theoretical framework for plant functional ecology. *Ecol Lett* 17:82–91.
42. Wong SC, Cowan IR, Farquhar GD (1979) Stomatal conductance correlates with photosynthetic capacity. *Nature* 282:424–426.
43. Farquhar GD, Ball MC, von Caemmerer S, Roksandic Z (1982) Effect of salinity and humidity on $\delta^{13}C$ value of halophytes—evidence for diffusional isotope fractionation determined by the ratio of intercellular/atmospheric partial pressure of CO_2 under different environmental conditions. *Oecologia* 52:121–124.
44. Battle M, et al. (2000) Global carbon sinks and their variability inferred from atmospheric O_2 and $\delta^{13}C$. *Science* 287:2467–2470.
45. Keeling RF, Manning AC (2013) Studies of recent changes in atmospheric O_2 content. *Treatise on Geochemistry*, eds Keeling RF, Russell L (Elsevier, Amsterdam), Vol 5, pp 385–404.
46. Khatiwala S, Primeau F, Hall T (2009) Reconstruction of the history of anthropogenic CO_2 concentrations in the ocean. *Nature* 462:346–349.
47. Campbell JE, et al. (2017) Large historical growth in global terrestrial gross primary production. *Nature* 544:84–87.
48. Ainsworth EA, Rogers A (2007) The response of photosynthesis and stomatal conductance to rising $[CO_2]$: Mechanisms and environmental interactions. *Plant Cell Environ* 30:258–270.
49. Wynn JG, Bird MI (2007) C4-derived soil organic carbon decomposes faster than its C3 counterpart in mixed C3/C4 soils. *Glob Chang Biol* 13:2206–2217.
50. Townsend AR, Asner GP, White JWC (2002) Land use effects on atmospheric ^{13}C imply a sizable terrestrial CO_2 sink in tropical latitudes. *Geophys Res Lett* 29:1–4.
51. Keller KM, et al. (2017) 20th century changes in carbon isotopes and water-use efficiency: Tree-ring-based evaluation of the CLM4. 5 and LPX-Bern models. *Biogeosciences* 14: 2641–2673.
52. Keeling CD, et al. (2001) *Exchanges of Atmospheric CO_2 and $^{13}CO_2$ with the Terrestrial Biosphere and Oceans from 1978 to 2000. I. Global Aspects* (Scripps Institution of Oceanography, San Diego), SIO Reference Series No. 01-06.
53. Rubino M, et al. (2013) A revised 1000 year atmospheric $\delta^{13}C$-CO_2 record from Law Dome and South Pole, Antarctica. *J Geophys Res Atmos* 118:8482–8499.
54. Friedli H, Siegenthaler U, Rauber D, Oeschger H (1987) Measurements of concentration, $^{13}C/^{12}C$ and $^{18}O/^{16}O$ ratios of tropospheric carbon dioxide over Switzerland. *Tellus B Chem Phys Meterol* 39:80–88.